Chapter 4

Holographically Recorded Low Spatial Frequency Volume Bragg Gratings and Holographic Optical Elements

Suzanne Martin, Hoda Akbari, Sanjay Keshri,

Dennis Bade, Izabela Naydenova, Kevin Murphy and

Vincent Toal

Additional information is available at the end of the chapter

http://dx.doi.org/10.5772/67296

Abstract

Low spatial frequency volume gratings (a few hundred lines per millimetre) are near the borderline of what can be considered Bragg gratings. Nevertheless, in some applications, their very low selectivity can be a benefit because it increases the angular and spectral working range of the holographic optical element. This chapter presents work carried out using an instantaneously selfdeveloping photopolymer recording material and examines holographic optical elements with spatial frequencies below 500 lines/mm. The advantages of volume photopolymer holographic gratings are discussed in the context of existing research. Specific examples explored include a combination of off-axis cylindrical lenses used to direct light from a solar simulator onto a c-Si solar cell, producing increases of up to 60% in the energy collected. A study of the microstructure of such elements is also presented. A good fit is obtained between the experimental and theoretical Bragg curves and the microstructure of the element is examined directly using microscopy. This is followed by a discussion of an unusual holographic recording approach that uses the nonlinearities inherent in low spatial frequency grating profiles to record gratings using a single beam. In conclusion, the properties of low spatial frequency volume gratings are summarized and future development discussed.

Keywords: Bragg gratings, low spatial frequency, photopolymer, holography

1. Introduction

Holographic optical elements (HOEs) are generally considered as either thin or thick gratings when their diffraction behaviour is modelled. Examples of thin gratings are commonplace because most commercially produced holograms, such as those on credit cards or banknotes, are surface relief holograms produced by a stamping process, and so the diffracting part of the structure is only a fraction of micron in thickness.

When a light beam passes through the grating, it obeys the classical grating equation given below, and orders are observed at the predicted angles

$$m\lambda = n\Lambda(\sin\alpha + \sin\beta) \tag{1}$$

where λ is the wavelength of light, Λ is the spatial period of grating, m is the order of diffraction, n is the refractive index of medium and α, β are the angles of incidence and diffraction, respectively.

Thick gratings, on the other hand, are usually volume gratings, distinct from surface gratings because the structures causing the diffraction are distributed through the full thickness of the material. Photopolymer gratings are one example. Some commercial photopolymer holograms have begun to appear on mobile phone batteries and other high value products. In these holograms, the refractive index variation is recorded through the full thickness, typically tens of microns, of the photopolymer layer. Light diffracted from this 'thick' Bragg structure also obeys the grating equation, but the greatest proportion of the light will be diffracted into the first order. This is because the light is effectively reflected from the planes of the fringes. This reflection combined with the grating equation gives the well-known Bragg condition which can be written as [1]

$$2n\Lambda\sin\theta = m\lambda \tag{2}$$

where θ is the angle of incidence.

The important factor determining whether 'thin' or 'thick' diffraction behaviour is observed is the size of the diffraction features in comparison to the thickness. Usually if the thickness of the recording material is smaller than the average spacing of the interference fringes, the holograms are considered to be thin holograms. The Q parameter, defined by Eq. (3), is derived from Kogelnik's equations for diffraction from volume gratings (discussed in the next section) and can be used in order to determine whether a hologram is 'thin' or 'thick' in its diffraction behaviour.

$$Q = \frac{2\pi\lambda d}{n\,\Lambda^2} \tag{3}$$

where λ is the wavelength, d is the thickness of the recording medium, n is the refractive index of the recording material and Λ is the fringe spacing.

Generally, gratings with the $Q < 1$ are considered thin gratings while those with values of $Q > 10$ are considered thick [2]. As can be seen from Eq. (3), for any given thickness and wavelength this depends on fringe spacing or spatial frequency. Low spatial

http://dx.doi.org/10.5772/67296

frequency volume Bragg gratings, having grating spatial frequency of typically a few hundred lines/mm, are on the borderline of what can be considered Bragg gratings, but at typical photopolymer thicknesses 30–50 μm, they can be considered Bragg gratings for visible wavelengths. In some applications, their low selectivity can be a significant benefit because it increases the angular and spectral working range of the HOE. In materials that perform well at low spatial frequencies, it is interesting to examine the characteristics and applications of HOEs with spatial frequencies below 500 lines/mm.

Volume phase holograms have advantages over surface relief holograms because of their high efficiency and resistance to surface contaminants. Applications include spectroscopy, astronomy and ultrafast lasers [3], as well as solar concentrators [4]. A number of different materials are available for recording them including silver halide, dichromatic gelatin (DCG), photoresists and photopolymers. The primary advantages of thick volume holograms over thin surface holograms are the possible high efficiencies (theoretically 100%) and the fact that most of the energy is diffracted into a single direction (order). For most applications where the hologram is expected to perform some or all of the functions of a conventional optical element such as a lens, maximum efficiency and minimum additional beams are advantageous. Beam splitting applications are an exception, of course. Photopolymers are useful materials because of their ease of use and potential for very high diffraction efficiency, but their key advantage in optical device applications is their self-developing capability, because it removes the need for chemical or physical processing after exposure. Assuming shrinkage is not a significant problem in the photopolymer used, the avoidance of chemical and physical processing is very important in maintaining the original photonic structure written in the volume of the material during the exposure/recording step. The longer term shelf life of the recorded devices varies according to the photopolymer used. In the acrylamide-based photopolymer used in the examples in this chapter, long-term stability of recorded gratings is good when the photopolymer layer is laminated with a protective plastic layer. Recent studies of the shelf life of such gratings sealed in plastic showed varied results however [5] pointing to the need for improved protection and alternative more robust formulations [6].

For thick gratings and elements, Kogelnik's coupled wave theory [1] is a widely accepted model that relates diffraction efficiency and angular selectivity of gratings to the grating's physical characteristics (thickness, spatial frequency and refractive index modulation).

According to Kogelnik, the diffraction efficiency (η) can be calculated using Eq. (4), allowing us to model how the diffraction efficiency varies with the angle of incidence, near the Bragg angle. This allows us to observe how grating thickness and spatial frequency affect the angular selectivity of an individual grating:

$$\eta = \frac{\sin^2\sqrt{(\xi^2 + \upsilon^2)}}{\left(1 + \frac{\xi^2}{\upsilon^2}\right)} \tag{4}$$

The parameters ξ and υ are defined as:

$$\xi = \Delta\theta\frac{kd}{2} \tag{5}$$

$$\upsilon = \frac{\pi n_1 d}{\lambda\cos\theta} \tag{6}$$

where d is the thickness of the grating, n_1 is the refractive index modulation, λ is the wavelength of the reconstructing beam, $\Delta\theta$ is the deviation from the Bragg angle and k is interference fringe vector, normal to the fringes with a magnitude $K = 2\pi$/spatial period. It can be seen from Eq. (4) that increasing the spatial period (reducing spatial frequency) is effective in controlling the angular selectivity. In materials where the refractive index modulation is small, significant thickness is required for high efficiency. Decreasing the spatial frequency (increasing the period) can be the better approach to control the angular selectivity as long as the gratings still behave as thick volume gratings [7].

2. Experimental arrangement for holographic elements

Holographic recording of diffractive optical elements involves careful spatial overlapping of two or more coherent beams so that the interference pattern they produce, once recorded into the material, will create a photonic structure capable of diffracting light in the desired way. For a simple diffractive device such as a two-way beam splitting element, the desired photonic structure may be a simple grating. For example, two coherent, collimated beams would be arranged to meet at the recording plane at a specific angle, producing a simple sinusoidal variation in intensity across, say, the horizontal axis of the recording medium. Once this is recorded in the material, a sinusoidal grating is produced which will act as a two-way beam splitter for a beam of the appropriate wavelength and incident angle.

The next step up in complexity is a shaped beam, such as a diverging beam, which when combined with the collimated reference beam produces an interference pattern consisting of a series of concentric rings. Once recorded, this pattern will produce a diffractive element with a similar variation in the refractive index, which, when illuminated correctly, produces a diverging beam. There are many types and variations of diffractive elements that can be produced in this way, especially when we consider recording with multiple beams, converging and diverging wavefronts, different inter-beam angles and different wavelengths. In this chapter, we discuss basic gratings and focusing/diverging elements with an angular offset.

The basic set-up for recording is shown in **Figure 1**; however, different adaptations are necessary for the work in each of the sections below. In order to make cylindrical lens elements, for example, a cylindrical lens is introduced into one of the interfering beams and for single-beam recording (Section 5) one beam is blocked completely during the second step. These alterations are mentioned in the relevant sections. Here, we show the standard optical arrangement for recording using the interference between two coherent beams.

The beam from a coherent laser source is spatially filtered, collimated and split in two and, after reflection of one of the beams of a plane mirror, the two beams are made to overlap at the photopolymer plate. The angle at which the beams meet can be altered by repositioning the mirror, allowing variation of the spatial frequency of the interference pattern and therefore the fringe period of the recorded grating. A grating has a single spatial frequency throughout, because two collimated beams are interfering so the inter-beam angle is constant across the polymer. The interference pattern at the photopolymer is recorded as a variation

http://dx.doi.org/10.5772/67296

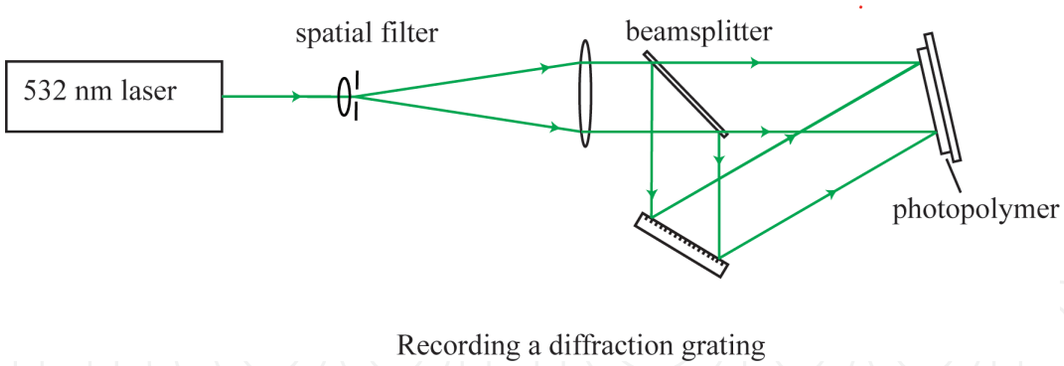

Figure 1. Basic optical arrangement for the recording of a holographic grating.

in the local refractive index inside the volume of the photosensitive material. The recording set-up includes a green laser of 532 nm wavelength, spatial filter, collimating lens, polarizing beam splitter, plane mirror, and for focusing elements, a conventional cylindrical lens (focal length 5 cm, ThorLabs, LJ182L2-A). The recording medium is the standard photopolymer used by researchers at the Centre for Industrial and Engineering Optics (IEO). It is an acrylamide-based formulation using acrylamide and bisacrylamide monomers, triethanolamine as the electron donor and polyvinylalchohol as the binder, as described elsewhere [7]. Layer thickness is controlled by the volume of liquid coating solution deposited on a known area of glass substrate.

3. Holographic low spatial frequency lens elements for light collection

The purpose of a diffractive solar collector is to gather sunlight from a large area and direct it onto a smaller area, where it can be converted to electric or thermal energy by, for example, using PV cells or thermal conversion. The advantage is that the light can be harvested cheaply from a larger area and the energy per unit area on the converter can be increased. As discussed previously, diffraction gratings can be used to change the direction of a light beam very efficiently, but they are only efficient over a small range of angles close to the Bragg angle, so they need to be used in combination if they are to be useful in collecting sunlight over most of the day.

Holographic optical elements (HOEs) have potential as solar concentrators because of their ability to diffract light at large offset angle and the potential for multiplexing a number of optical components in the same layer. Recent research has demonstrated different holographic elements in a variety of arrangements for solar applications to make diffractive elements that will re-direct and focus incoming light to the desired line using (cylindrical HOE) or spot (spherical HOE) for conversion [8–12].

A large number of researchers have demonstrated novel designs, for example, a planar concentrator using a low-cost holographic film that selects the most useful bands of the solar spectrum and concentrates them onto the surface of the photovoltaic cell, has been demonstrated by Kostuk et al. [13], and Sreebha et al. [14] have reported results on transmission holographic

optical elements recorded in a silver halide material. Bianco et al. have recently reported successful concentration of solar light using an array of three spherical lenses recorded in a sol-gel photopolymer [15].

Photopolymers are excellent materials for producing such diffractive elements, being thin, lightweight, inexpensive and highly efficient, but challenges remain in reducing the angular selectivity of these relatively thick layers and in applying the technology to natural light in real-world applications.

High-efficiency diffractive optical elements have been recorded and multiplexed in photopolymer materials previously for this and other applications [16, 17]. Previous work by the authors addressed the issue of increasing the angular working range in photopolymers and demonstrated photopolymer spherical and cylindrical focusing elements that had very high efficiency when measured with monochromatic, linearly polarized laser sources [18]. In this section, the combination of pairs of elements with the same focus is demonstrated in photopolymer and tested with a solar simulator.

For these experiments, the electrical characterisation was carried out by measuring the current-voltage (*I-V*) characteristics of c-Si solar cells (Solar capture Technologies) with and without the DOE placed in front of the cell in such a way as to re-direct and focus additional light onto the solar cell. *I-V* measurements were performed using an Keithley 2400 SMU (source meter unit) with a LabVIEW interface, using the set-up shown in **Figure 2**. The light source used was a metal halide discharge lamp (Griven, GR0262).

The distance between the HOE and the silicon cells was the same as the focal length of the HOEs which in this case was 5 ± 0.1 cm. This arrangement tests the effect of two DOE elements; however applications could involve arrays of such elements surrounding the cell, each contributing additional light.

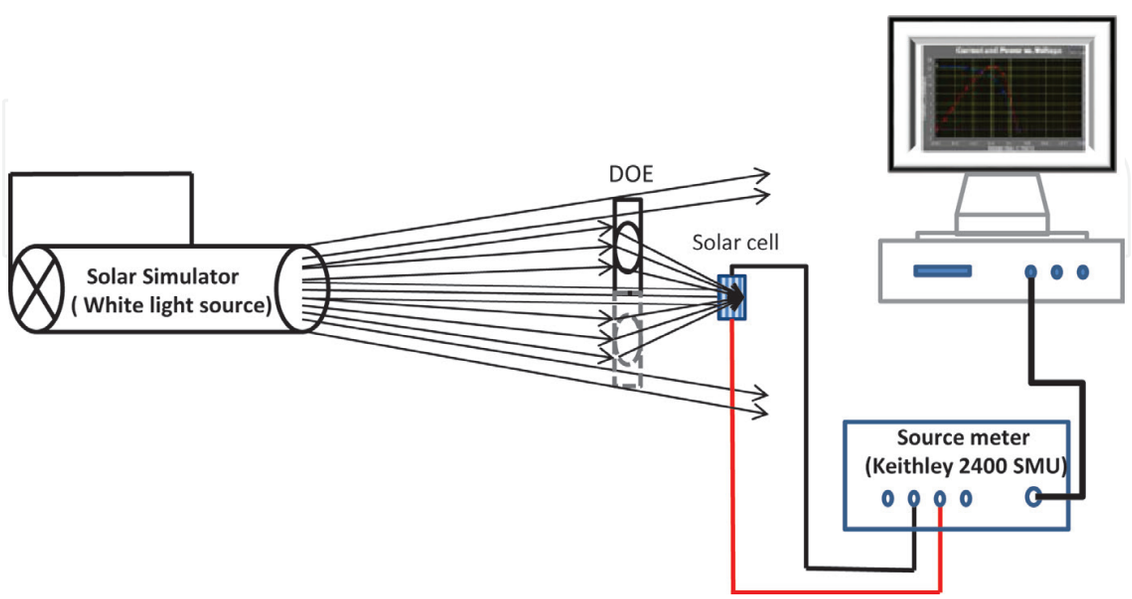

Figure 2. Diagram of the experimental setup for electrical measurements.

http://dx.doi.org/10.5772/67296

3.1. Recording high efficiency diffractive optical elements at low spatial frequency

Focusing HOEs were made by interfering a beam focused by a cylindrical lens beam with a collimated reference beam and placing the photopolymer layer at the area of overlap using the basic holographic set-up described in the experimental section. In such off-axis focusing DOEs, the spatial frequency of the grating planes will vary across the DOE, as will be discussed in the next section. In this example, the minimum and maximum spatial frequencies were 112 and 485 lines/mm, respectively.

A range of HOEs with an off-axis focusing effect was recorded in order to demonstrate that high efficiency could be achieved with low spatial frequency elements. Diffraction efficiency at Bragg incidence is over 95% (corrected for reflection at front and back surfaces). **Figure 3** shows how the diffraction efficiency changes with the angle of incidence. The full-width half-maximum (FWHM) is approximately 4°, which is a significant improvement on the working range for higher spatial frequencies [18]. The data were obtained by mounting the grating on a rotation stage keeping the laser and detector fixed.

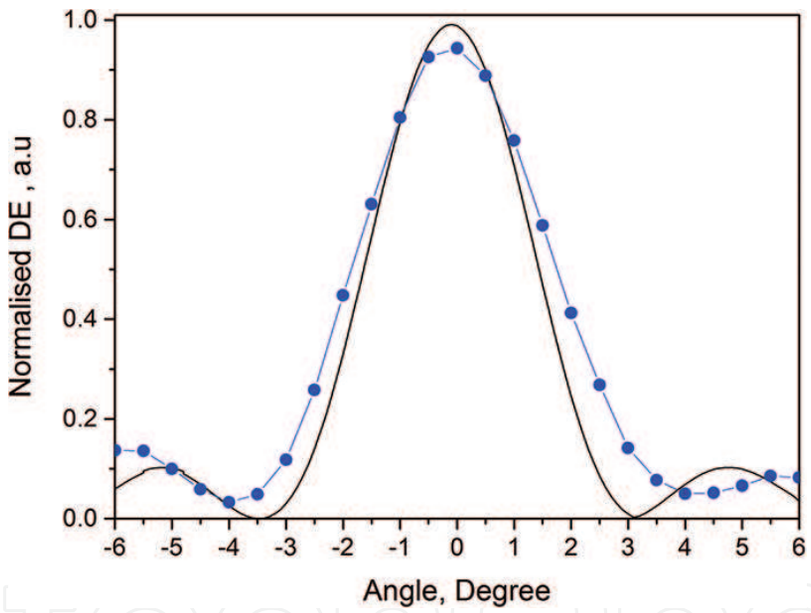

Figure 3. Diffraction efficiency versus angle for a cylindrical DOE at central spatial frequency of 300 lines/mm and recording intensity of 1 mW/cm². The dotted line shows the measured values and the smooth line is the theoretical curve for a 300 lines/mm volume grating of this diffraction efficiency in a 50 micron thick photopolymer layer.

3.2. Investigating the potential for multiplexing by stacking: three gratings with different slant angles

Photopolymer gratings were recorded with three different slant angles. **Figure 4** shows plots of the percentage of light falling on the fixed detector as the angle of incidence of the light is varied for the three individual gratings before stacking them together. In each case, the grating is fixed relative to the detector and only the angle of incidence is varied. This mimics the function of a passive (non-tracking) solar cell. The detector collects the light that would fall on

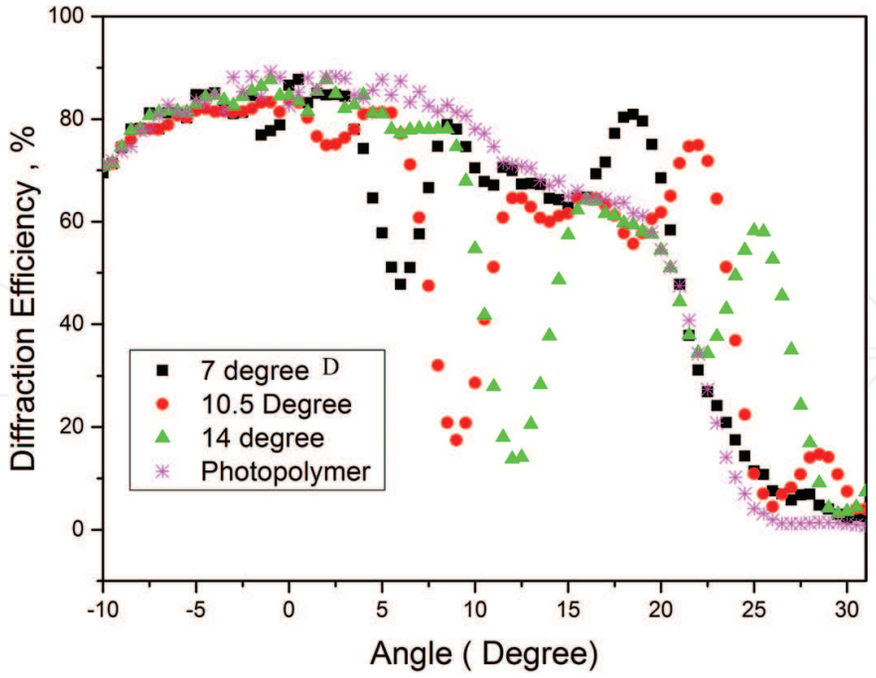

Figure 4. The variation of the percentage of light falling on the detector with angle of incidence for three individual gratings recorded at different slant angles with a spatial frequency of 300 lines/mm in layers with thickness of about 50 μm; the recording intensity was 1 mW/cm². A photopolymer layer with no grating is included for comparison.

the cell with and without the gratings in place. The 'photopolymer' line shows the variation in intensity at the detector without the presence of any grating (just a layer of clear photopolymer) for comparison. From these results, redirection of the incident beam by the gratings can clearly be observed at the appropriate angles. Light incident at over 25°, which would have otherwise missed the detector (or solar cell in a real application) is very efficiently captured using the gratings. However, a key issue is highlighted here. As well as directing the light from higher angles to a lower angle, each grating will also do the reverse. This is caused by the fact that each grating has two angles for which the light is 'on Bragg' for diffraction (corresponding to the two beams with which the grating was recorded).

The angular selectivity of the stack of the three gratings laminated together was then measured using the same method. The results are shown in **Figure 5**. The same effect was observed for the stacked device as in **Figure 4**. The results confirm that this method has improved the angular working range of the device. However, efficiency is reduced at the lower angles so that there is no net gain. Diffraction from higher angles would appear to be most useful in circumstances where the grating is offset from the main path to the solar cell, such as off-axis DOEs, in this way the direct light is unaffected, but the grating can usefully divert light from higher angles onto the solar cell.

3.3. Use of a combined device to increase the concentration ratio of solar cells

An alternative arrangement is to use off-axis elements to increase the area from which light is collected and focused onto the solar cell, thereby increasing the energy at the cell. For maximum concentration, the DOEs should be recorded so that their focal points overlap. Low

http://dx.doi.org/10.5772/67296

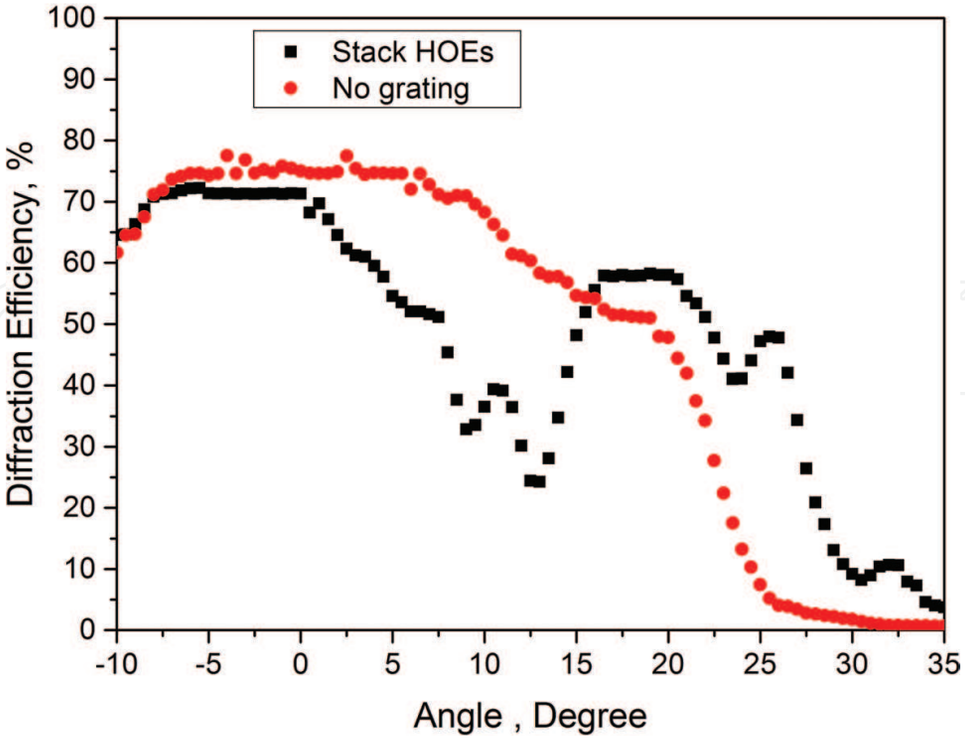

Figure 5. The variation of the percentage of light falling on the detector with angle of incidence for a stack of three laminated gratings (from **Figure 4**) and a clear photopolymer layer with no grating.

spatial frequency elements are used so that the wavelength selectivity is low and the elements can focus the full spectrum of white light onto the same solar cell. Tests were carried out using a solar simulator and a Si solar cell.

The current I, as a function of voltage applied, V, across the c-Si solar cell, was measured and the I-V curve was obtained (**Figure 6**). In this experiment, the area of the DOE was kept constant at 113 mm^2. In **Table 1**, I_{sc} represents the short circuit current for the solar cell, which is the maximum possible, produced when the cell impedance is low and is calculated when the voltage equals zero, i.e. at $V = 0$, $I = I_{sc}$. The short circuit current is due to the generation and collection of light-generated carriers within the cell. For an ideal solar cell, the short circuit current and the light-generated current are identical for moderate resistive loss. Therefore, an increase in the short circuit current is a reliable indicator of an increase in the light-generated current. J_{sc} is the short circuit current density, defined as $J_{sc} = I_{sc}$/area of the cell.

The short circuit current (I_{sc}) output of the reference cell, without the DOE in place, was approximately 3.7 ± 0.1 mA. When a single cylindrical DOE was included, an increase in I_{sc} of 16% was observed.

This measurement was then carried out for an array of two cylindrical DOEs, which resulted in an increase in the I_{sc} of 40%. These results suggest that the use of larger arrays of cylindrical and/or spherical DOEs can achieve higher relative increase in I_{sc} for smaller areas of solar cells. The value for the short circuit current density (J_{sc}) of the Si solar cell was estimated using the I-V data for a single cylindrical DOE and a pair of DOEs for a solar cell of area 60 mm^2. The results are presented in **Table 1**.

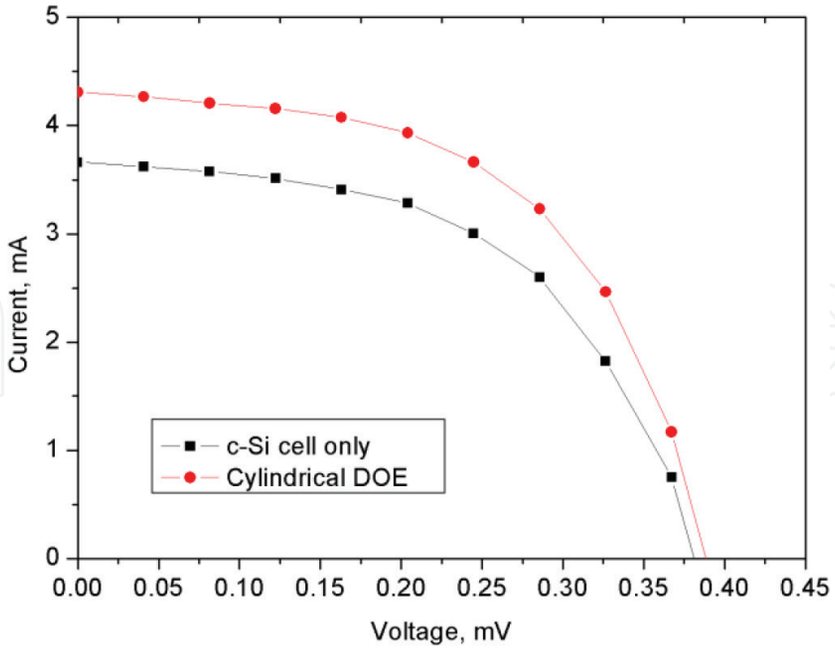

Figure 6. *I-V* curves for a c-Si solar cell (area = 60 mm^2) with and without a cylindrical DOE in place.

	I_{sc} **mA/cm^2**	ΔI_{sc}	ΔI_{sc} % **±0.03**	J_{sc} **mA/cm^2**
Si cell	3.7			0.061
With cylindrical DOE	4.3	0.6	16	0.071
Array of two cylindrical DOE	5.2	1.5	40	0.086

Table 1. Calculated J_{sc} of the Si solar cell with a range of DOEs. I_{sc} is the short-circuit current and J_{sc} is the short circuit current density.

Figure 7 presents the relative increase in the I_{sc} for the c-Si solar cells versus the area of the solar cells. The illuminated area of the DOE remained constant at 113 mm^2 throughout the experiment while the solar cell area was varied between 9 and 100 mm^2. In order to optimize the concentration ratio, the preference is to use solar cells significantly smaller than the DOEs. These results show that there is a significant improvement in the output current obtained when using the holographic focusing elements.

It has been observed that for solar cells with an area of 9 mm^2, a 34% increase in the output current is achieved with a single DOE compared to 10% for a 100 mm^2 solar cell. This is because the smaller cell area makes better use of the focusing effect.

The relative increase for an array of two cylindrical DOEs was nearly double that of single cylindrical DOE. The device is capable of collecting light from a large incident angle and

http://dx.doi.org/10.5772/67296

redirecting it onto the centre of the solar cell. Photographs of the light spots diffracted from holographically recorded diffractive lenses are shown in **Figure 8**. The first photograph shows a collimated green laser beam (circular spot) which is brought to a line focus by the DOE on the left of the picture. Additional beams to the left and right of these are also observed in the photograph; however, in reality they are very weak. Experimentally, for off-axis focusing DOE lenses, more than 90% of the incident light is typically measured in the focused beam. The second image in **Figure 8** is a photograph of the transparent diffractive lens viewed in room lighting.

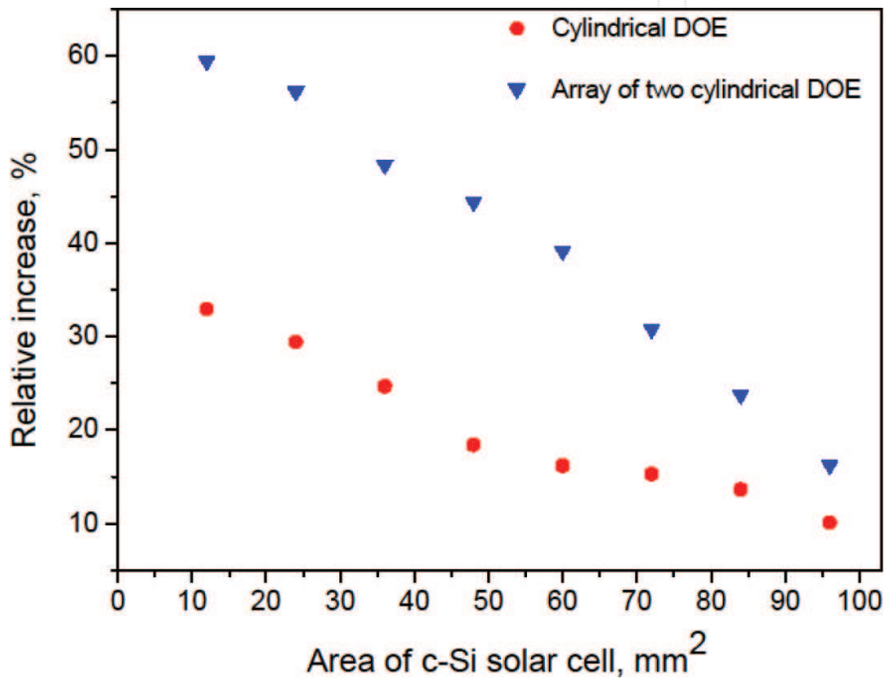

Figure 7. The percentage increase of output current of c-Si solar cells versus area of the c-Si cells for a single cylindrical DOE and an arrangement of two cylindrical DOEs.

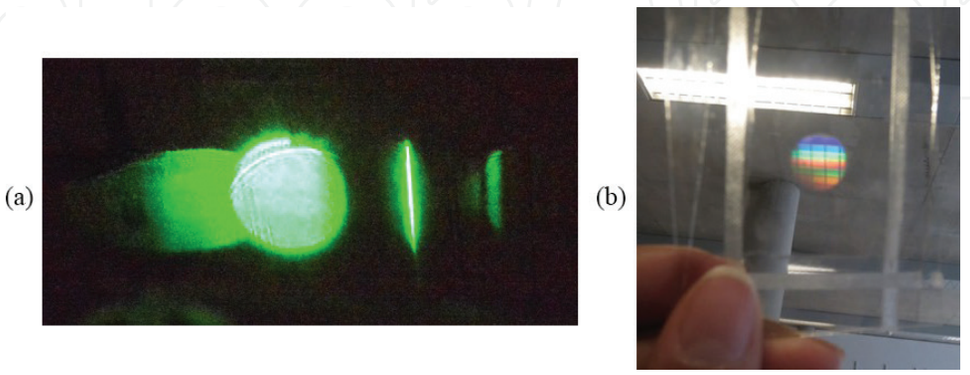

Figure 8. Photographs of the light diffracted by holographic lenses recorded in acrylamide photopolymer (a) illuminated with an expanded laser beam and (b) in room light.

4. Analysis of the photonic structure of low spatial frequency lens elements

Volume phase holographic (VPH) gratings can be recorded on different types of materials such as silver halide, dichromatic gelatin (DCG), photoresists, photopolymer, etc. However, photopolymer provides certain advantages [19] such as higher efficiency, self-development and cost effectiveness. In general, VPH gratings follow Bragg's law [20] for the propagation of light inside a volume in which periodic modulation of the refractive index forms the grating structure. In certain circumstances, for example thicker media, VPH gratings recorded at low spatial frequency can also be considered as Bragg gratings and they increase the angular and spectral range of VPH gratings [18]. In this section, we examine the photonic structure of the recorded lenses using microscopy in order to verify the model used to design the lens and calculate the spatial frequency and slant angle of the grating pattern at specific points on the recorded lens. We also use Kogelnik's coupled wave theory (KCWT) to predict the expected Bragg curves and compare them to the curves obtained experimentally measured at these locations.

The lens elements are recorded as described above by including a focusing lens into one arm of a standard two-beam optical arrangement for holographic recording at 532 nm. In this section, the analysis of the local diffraction behaviour using an unexpanded 633 nm laser beam and measuring the Bragg curve (intensity variation in the diffracted beam as the grating is rotated though a range of angles) is complemented by microscopic imaging at the same location.

4.1. Modelling the recorded holographic optical element

The focusing elements studied were 5 cm focal length off-axis cylindrical lenses, so the micro-structure was expected to vary significantly laterally across the recorded element. **Figure 9** shows a schematic of the recording arrangement. Clearly the angles at which the interfering beams meet varies from left to right and we would expect both slant angle and spatial frequency of the grating pattern to change.

Simple geometry allows us to calculate the inter-beam angle (which determines the spatial frequency) and the slant angle, i.e. the angle between the bisector of the angle between the two beams (inside the medium) and the normal to the recording plane). Since the lens is not spherical in this example there is no variation vertically (out of the plane of the page in **Figure 9**). The Bragg angle θ_o is related to the fringe spacing (Λ) recorded in the hologram by the relation

$$\sin \theta_o = \frac{\lambda}{2\Lambda} \tag{7}$$

In this work, we use equation (7) to predict the grating structure and verify it experimentally at three specific locations on the element, the centre and points 3 mm either side of the centre. For any local position across the element, the slant could be calculated using the recording geometry and compared to the experimentally observed position of the peak in the Bragg curve. Equally, the local grating period was calculated from knowledge of the inter-beam angle at that specific location during recording and this was compared with microscopic imaging results.

http://dx.doi.org/10.5772/67296

The shape of the Bragg curve was then modelled using those parameters in KCWT, and fitted to the experimental data (normalised to the measured diffraction efficiency value). **Figure 10(a)** shows the calculated spatial period across the lens element. The inverted red triangles show the measured values obtained from the microscopy images, which are 2.66, 3.37, 6.59 μm at left, centre and right, respectively (left, right are 3 mm away from centre). **Figure 10(b)** shows the calculated slant angle at positions across the element.

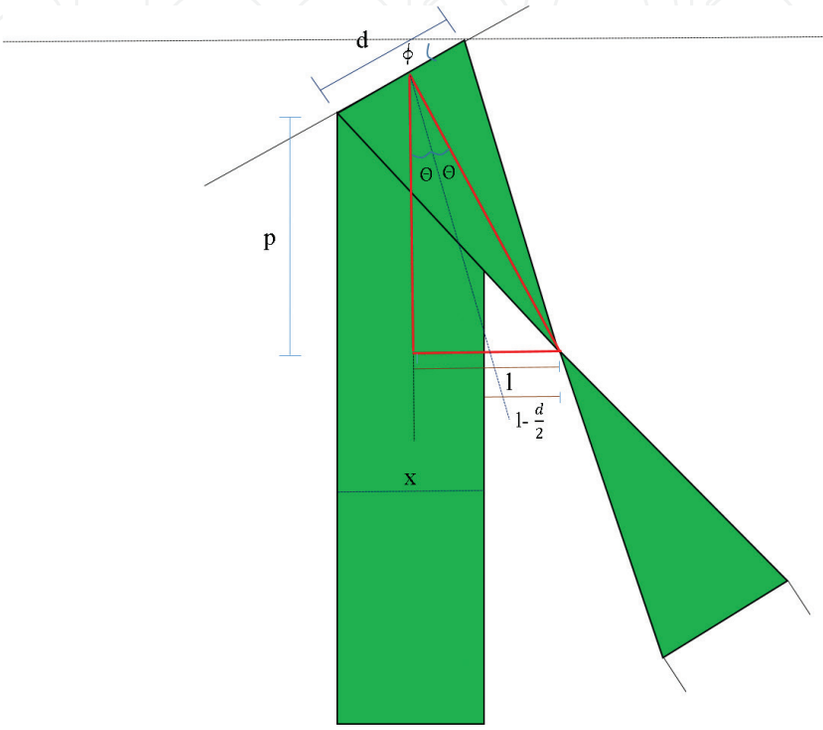

Figure 9. Schematic illustration of the geometry of the recording set-up showing the angles at which the interfering beams meet at the photopolymer plate of width d, at a slant angle ϕ.

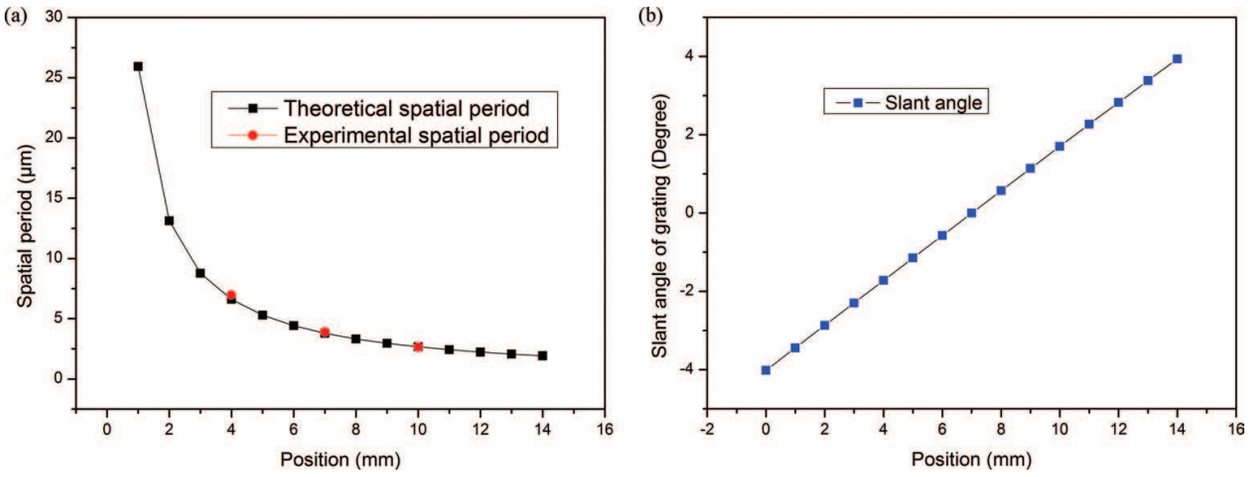

Figure 10. (a) Spatial period across the VPH lens: 0 corresponds to the right side and 14 corresponds to the left side of the lens and (b) slant angle across the VPH lens.

4.2. Local microstructure and diffraction behaviour

Figure 11 shows the experimental intensity data obtained by illuminating the three positions with an unexpanded 633 nm He-Ne beam and varying the angle of incidence. As expected, the three curves are shifted relative to one another, verifying that each location has a different slant angle and inter-beam angle. Each curve has a different FWHM because of the different grating periods.

The curves are fitted to theoretical curves generated by putting the parameters calculated using the geometry into the KCWT equations and setting the wavelength to 633 nm.

As can be seen from the figure very good agreement is obtained. The small broadening of the Bragg peaks can be accounted for by the fact that the incident beam had a finite width, and so in reality the result is not for a specific location but for an average over the beam width. The thickness of the photopolymer used was 70 ± 5 μm and was measured by white light interferometry.

In order to verify the theoretical calculation of spatial period of grating, the microscopic image of the gratings has been taken using a phase contrast microscope (Olympus DP72) at three different positions, centre and 3 mm away from the centre (right and left). These are shown in **Figure 12**. The spatial periods measured using the microscope are 2.6 ± 0.1, 3.9 ± 0.1 and 7.0 ± 0.1 μm at left, centre and right of the VPH cylindrical lens, respectively. The theoretical values for these positions can be seen from the graph of **Figure 12(a)** and are 2.66, 3.37, 6.59 μm, respectively.

It can be observed that the holographic recording has produced the predicted diffraction grating patterns. The experimental results for the diffraction characteristics of the local pattern fit well with the theoretical predictions for these spatial frequencies made with KCWT. A small

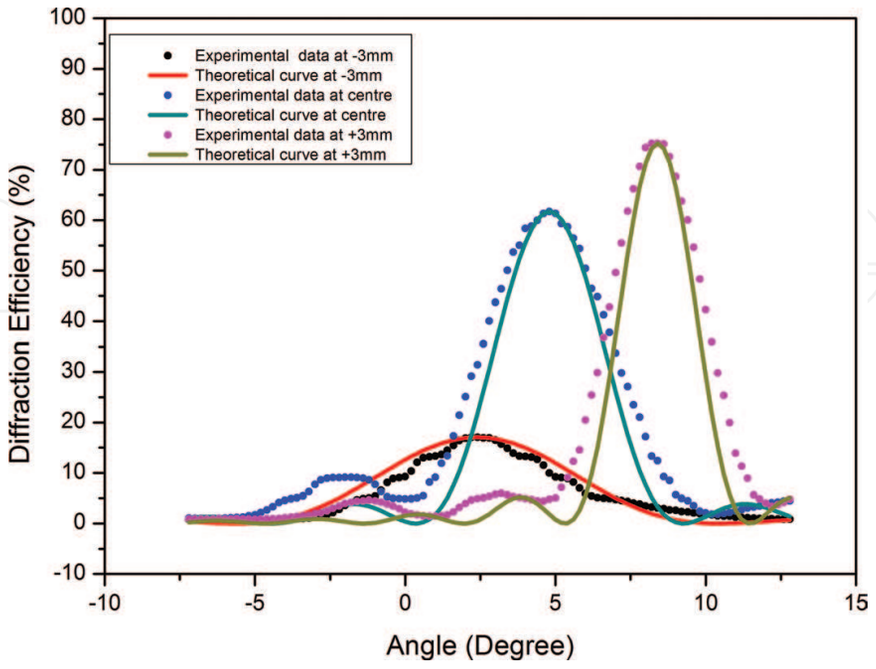

Figure 11. Theoretical and experimental angular selectivity curves for three different positions (centre and 3 mm left and right of centre) on the VPH cylindrical lens.

http://dx.doi.org/10.5772/67296

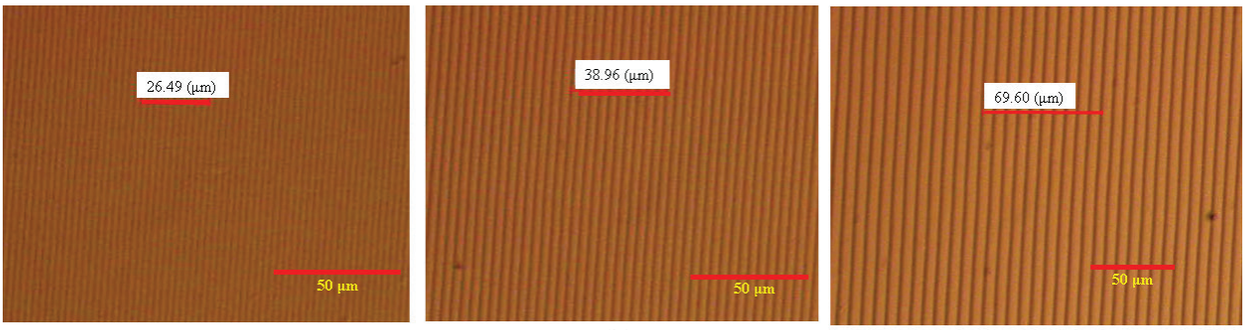

Figure 12. Microscopic image of the surface structure of the holographic lens at the (a) left position (3 mm from centre), (b) centre and (c) right position (3 mm from centre).

amount of broadening is observed in the experimental curves, but this is probably due to the size of the probe beam, beam walk off or scattering. The spatial periods obtained from the microscopic images agree with the theory, and it can be seen from the microscopic images that the spatial period is increasing from left to right of the VPH cylindrical lens. Future work will involve fabricating and modelling lens elements at different wavelengths.

5. Writing gratings with a single beam

Most standard holographic recording is, of course, achieved by interfering two coherent recording beams. The interference pattern they create is recorded in the medium as a diffractive structure in the medium. However, due to the challenges of stability and size associated with splitting and recombining beams, various methods have been employed in order to achieve recording with a single beam.

Early work by Kukhtarev et al. [21] demonstrated holographic recording using only one input beam in a photorefractive $BaTiO_3$ crystal using the photogalvanic coupling between orthogonal birefringent modes. Later, Naruse et al. [22] multiplexed ten gratings into a Fe-doped $LiNbO_3$ crystal with a single recording beam. They used the crystal edge in a wavefront splitting arrangement. Mitsuhashi and Obara [23], using a similar approach, demonstrated a compact holographic memory system using a single-beam geometry in Fe-doped $LiNbO_3$. At that time, they estimated a maximum total capacity of 23 GB based on beam diameter of 5 mm in a system using 635 nm light and a 10 mm crystal using both angular and spatial multiplexing. More recently, Yau et al. [24] have proposed another method that uses a single object beam to record images in a photorefractive $LiNbO_3$ crystal which allows imaging through a dynamically varying medium. Chiang et al. proposed a method that uses a single object beam to record multiple images in a medium without the need for a reference wave using a lenticular array [25]. This was demonstrated by recording four holograms in a $30 \times 30 \times 1$ mm^3 Fe-doped $LiNbO_3$ crystal with a single exposure.

Recent work by Kukhtarev and Kukhtareva develops a dynamic version of the early single-beam recording system, demonstrating dynamic holographic interferometry [26] and also holographic amplification of weak images without phase distortions [27].

In the commercial arena, Optware, a Japanese-based company, developed a new method of holographic storage called collinear holography. Instead of separate signal and reference beams to create the interference pattern, Optware are using a collinear approach by aligning the two laser beams into a single beam of coaxial light to create data fringes. This approach significantly simplified the recording set-up [28]. Optware released a prototype of this recording system operating at a wavelength of 532 nm with an overall storage capacity of 200 GB on a recording medium with a diameter of 120 mm (HVD Pro Series 1000). They also released a credit card-sized layer with a storage capacity of 30 GB and demonstrated a recording system with a storage capacity of 1 TB with a data transfer rate of 128 MB/s.

An example of the single-beam recording method described here was first reported by the authors in 1998 [29]. After first recording, weak diffraction gratings in the photopolymer were illuminated on Bragg, with just one of the recording beams. For gratings with initial diffraction efficiencies ranging from less than 1% to 64%, a further increase in diffraction efficiency was observed during the single-beam exposure. For example, a grating with 7.5% efficiency was observed to increase to 60% efficiency over several minutes of single-beam exposure. It was suggested at the time that the increase may be caused by either uniform polymerization of unreacted monomer in the grating, as had been observed in other photopolymers [30], or diffraction from the recorded grating. Further work [31] showed that the grating strength only increased significantly when the single writing beam was incident close to the Bragg angle of the pre-recorded grating.

In this section, this method of writing holographic gratings using weak pre-recorded gratings is explored further, because of its potential to allow the use of just one beam at the data writing stage. New gratings, angularly separated from the pre-written grating, are written using a single beam and the dependence on grating thickness is demonstrated. We demonstrate that this approach allows the writing of high diffraction efficiency gratings in unstable conditions due to the fact that the second beam is generated from within the photopolymer layer, in a manner similar to beam pumping in photorefractive crystals. We demonstrate that angular multiplexing is also possible, allowing one grating to be amplified without amplifying the other pre-recorded gratings.

5.1. Holographic recording process

A two-step process was used: (1) recording the weak 'seed' gratings with two recording beams and (2) exposure of the seed grating to one beam. There was a short delay between the two steps, during which both beams were blocked.

5.1.1. Two-beam recording

The first step was to record a grating, usually with a diffraction efficiency of approximately 1%, in the photopolymer medium. A standard holographic grating recording arrangement was used, with two coherent interfering beams (532 nm) using beam splitters and mirrors, as shown in **Figure 1**. The arrangement is for unslanted gratings. A He-Ne beam (633 nm) was used to monitor the diffraction efficiency throughout the initial recording and subsequent illumination. This was possible because, in the formulation used, the photopolymer is not sensitive to

http://dx.doi.org/10.5772/67296

red light. A short exposure time (around 1 sec) was used for the initial recording in order to keep the efficiency of the initial grating low. The spatial frequency was controlled by adjusting the angle between the two interfering beams and is 500 lines/mm in the work reported here.

5.1.2. Single-beam recording

The next step was to illuminate the grating on Bragg, with a single beam and observe the change in diffraction efficiency. The simplest way to do this was to use an additional shutter to block one of the two recording beams. Usually a short interval with no writing beam illumination was allowed after the initial grating recording in order to allow the system to record any spontaneous change that may be occurring in the absence of illumination. Exposure times and writing beam illumination were controlled using Uniblitz electronic shutters. The photopolymer grating was mounted on a rotation stage so that angles of illumination could also be varied.

5.2. Single-beam holographic recording results

Figure 13 shows the diffraction efficiency changing during a typical exposure starting with a standard two-beam holographic recording of 2 sec followed by a 25 sec delay, during which there is no illumination. Then, at 27 sec, illumination with one of the writing beams commences. The diffraction efficiency increase obtained during the single-beam exposure is significant and diffraction efficiency of the final grating is much higher than at the point when single-beam exposure commences. In this case, the grating spatial frequency is 500 lines/mm, and the layer thickness is 135 μm. Each exposing beam has an intensity of 2.5 mW/cm^2. **Figure 13** shows typical diffraction efficiency increase observed upon exposure to a single on-Bragg recording beam. No dependence was found on the delay time between the two beams and single-beam exposure and weak gratings could be enhanced by single-beam exposure after 12 weeks, as long as the photopolymer was still sensitive.

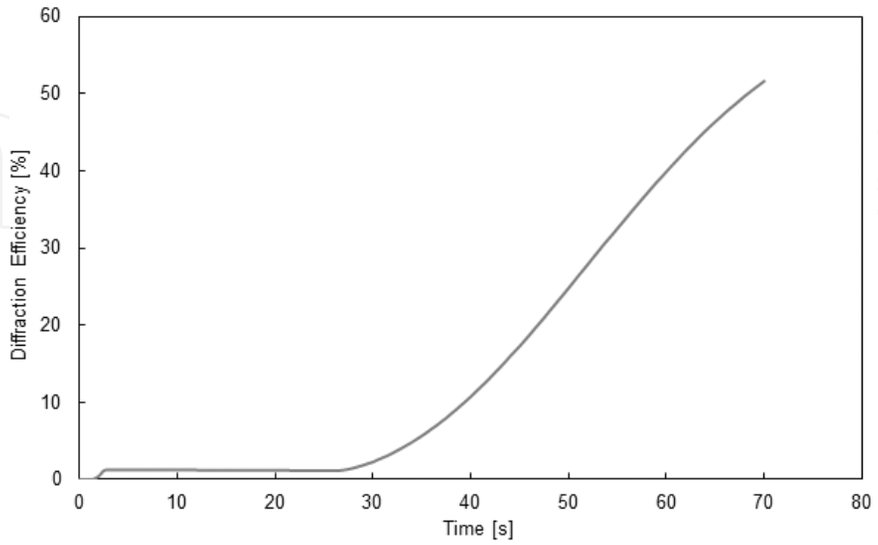

Figure 13. Diffraction efficiency versus exposure time. A standard two-beam holographic recording of 2 sec is followed by a 25 sec delay (no illumination) and then illumination with just one of the writing beams. Exposure intensity is 2.5 mW/cm^2 in each beam.

The increase in diffraction efficiency consistently observed under single-beam illumination in this photopolymer is due to a new grating formed by the interference between the single writing beam and the first-order beam generated by diffraction at the pre-recorded weak grating (see discussion below).

5.2.1. Single-beam recording with Bragg mismatch

The need for near-Bragg matching of the single writing beam rules out any bulk photochemical effect as the cause of the diffraction efficiency increase, supports the idea that diffraction is the main contributor. In order to study this further, and also assess the potential for multiplexing, the angle of incidence of the single writing beam was varied around the Bragg angle of the pre-recorded grating. The results are shown in **Figure 14**. The original seed grating diffraction efficiency was close to 1% in each case and the photopolymer thickness was 200 μm. The spatial frequency of the seed grating was 500 lines/mm. It can be seen from **Figure 14** that there is an optimum angle, close to the Bragg angle of the pre-recorded grating, that maximizes the strength of the grating recorded with the single-beam writing process. As the illuminating beam is moved further away from the optimal angle, the final diffraction efficiency is reduced under the same exposure conditions. This is probably due to the reduced coupling

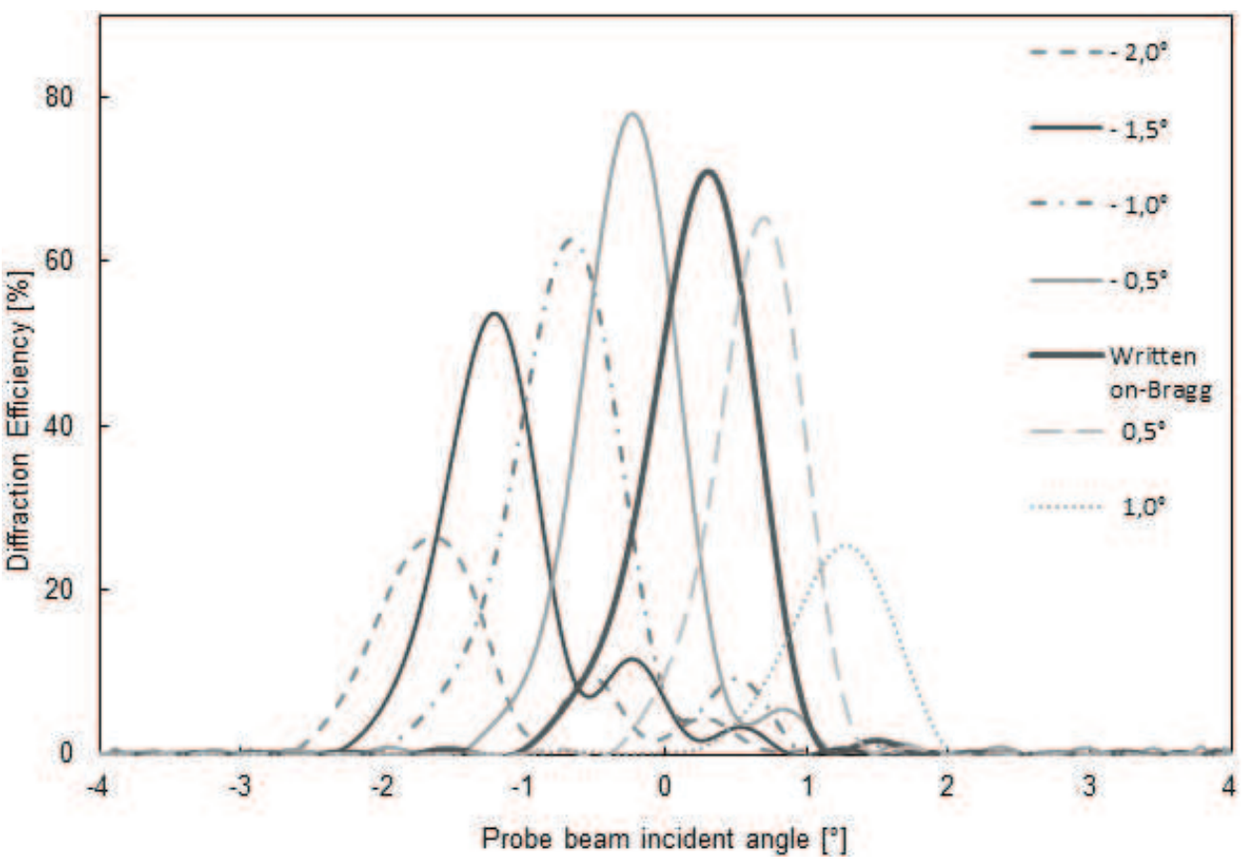

Figure 14. Bragg curves (the variation of diffraction efficiency with reading beam angle of incidence) for a series of gratings formed using the single beam process, using different angles of incidence of the single writing beam. The layer thickness is 200 μm. The arrows indicate the offset (in degrees) from the Bragg angle of the seed grating (0°).

http://dx.doi.org/10.5772/67296

between the single writing beam and the seed grating. In this example, the optimal angle is about 0.5° from the Bragg angle for the original grating. The asymmetry of the sidelobes is also a consistent feature. Both of these are thought to be due to fringe bending during the formation of the grating under single-beam exposure as discussed below.

This work demonstrates that the grating strength only increases significantly under single-beam illumination when the single writing beam is incident close to the Bragg angle of the pre-recorded grating.

As discussed in Ref. [31], the angular position of the Bragg peak for the gratings recorded in this way is linearly dependent on the angle of incidence of the single writing beam. This shows that the formation of a new grating formed by diffraction is responsible for the observed increases.

We propose that the weak diffracted beam interferes with the undiffracted beam to produce a low-contrast interference pattern which is immediately recorded in the material. If the new grating is in phase with the original grating, more light will then be diffracted into the weaker beam, reducing the beam ratio and increasing the contrast in the interference pattern, in turn producing an even stronger diffracted beam. In this way, quite weak gratings can rapidly 'seed' the growth of relatively high diffraction efficiency gratings. This growth of a new grating is analogous to the energy transfer between the strong beam and the weak beam in 'beam pumping' in photorefractive crystals, except that the refractive index modulation created is permanent.

A potential difficulty with the above explanation is the phase mismatch between the 'seed' grating and any grating created by diffraction at the 'seed' grating. This is due to the fact that there will be a phase difference ($\pi/2$) between the incident beam and the beam diffracted by the phase grating, which would cause any new grating to be out of phase with the original. Beam pumping in photorefractives, which is also initiated by diffraction at a weak grating, occurs only because the recorded grating in photorefractive crystals is laterally displaced with respect to the interference fringes that create it.

Unlike photorefractive crystals, photopolymers are usually considered to produce gratings that are not laterally shifted from the interference pattern that creates them. Thus we might not expect the interference pattern created by the incident beam and its diffracted beam to produce a grating that is in phase with the one that created it. However, such shifts and non-linear recording profiles have been observed in holographic recording materials such as acrylamide photopolymers [32], nanoparticle-doped photopolymers [33] and silver halide emulsions [34]. Murciano et al. [35] reported that effects such as beam bending and two wave mixing have been observed even with very small phase shifts, by them and other authors in similar materials. They analysed the origin and effects of fringe bending and Bragg detuning in holographic gratings recorded in rigid media such as photopolymerizable inorganic silica glass materials and proposed that they occurred as a result of the non-sinusoidal nature of the recorded pattern. Using an acrylamide photopolymer-doped sol gel, Murciano et al. observed two-wave mixing during two-beam recording and used a two-wave mixing model to explain the asymmetry and angular shift (fringe bending) observed in their angular selectivity (Bragg) curves. The reconstruction model used by Murciano et al. to analyse the gratings used coupled wave theory taking into account two wave mixing occurring during recording. Fringe

bending becomes larger as thickness and refractive index modulation increase and, of course, depends greatly on the initial beam ratio. Good agreement was obtained between experimental and theoretical results of simulations with a shift of just 2.6° between the recorded grating and the light pattern, demonstrating that very small shifts can cause such effects.

It seems likely that our results described above would have a similar origin. That is the non-sinusoidal refractive index profile of the recorded grating provides enough of a phase shift to allow coupling from the strong beam to the weak diffracted beam during single-beam recording. It should also be borne in mind that the beam ratio is very large (typically 99:1) at the start of the single-beam recording step, so small amounts of energy transfer from the strong beam will have a significant effect and the fringe period is very much larger than the wavelength for these low spatial frequency gratings. In the case of these acrylamide-based photopolymers, gratings are recorded via photopolymerization and diffusion. Either of these processes can dominate depending on the recording intensity, spatial frequency and photopolymer formulation [36], and non-sinusoidal grating profiles are also common especially at low spatial frequencies [37]. It has been observed that the process of enhancing diffraction efficiency reported here is stronger at lower spatial frequencies.

5.2.2. Single-beam recording with different layer thickness

Experiments with different layer thicknesses ranging from 60 to 240 μm showed that the enhancement of the seed grating occurs much more in thicker layers. **Figure 15** shows the diffraction efficiency increasing under single-beam illumination from an initial diffraction efficiency of approximately 1% for thicknesses of 60, 130, 190 and 240 μm. These curves are each obtained in the same way as that in **Figure 13** but the delay between the two exposures was 110 sec in these experiments. The gratings were exposed to a single beam at the Bragg angle for 150 sec. The spatial frequency is 500 lines/mm and each exposing beam has an intensity of 2.5 mW/cm^2. It is observed that the increase in efficiency when recording with a single beam is much more pronounced in thicker layers and practically non-existent in the layer with thickness 60 μm It is probable that this dependence is due the increased distance over which energy can be transferred from the weaker beam to the stronger beam, as described above.

5.2.3. Single-beam recording at different spatial frequencies

Figure 16 shows the Bragg curves of a number of single-beam gratings recorded at different spatial frequencies. Although the diffraction efficiency of the 'seed' grating was approximately 1% in each case and the single-beam recording time is 30 sec for all gratings, a significant dependence on grating spatial frequency is observed. In this instance, the recording intensity is 1.8 mW/cm^2. The initial exposure time with two beams was 1 sec for 2000 and 1500 lines/mm and 0.75 sec for 1000–250 lines/mm in these examples but the diffraction efficiency was close to 1% in each case.

The pronounced increase observed for lower spatial frequencies indicates that fringe period may be a crucial factor. It was suggested above that the non-sinusoidal refractive index profile of the recorded grating could provide enough of a phase shift to allow coupling from the strong

http://dx.doi.org/10.5772/67296

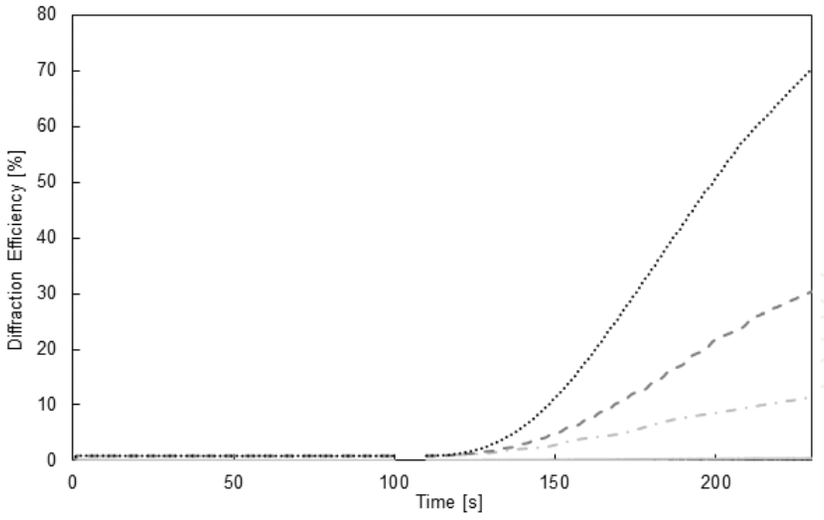

Figure 15. Growth in diffraction efficiency, under single beam illumination, of 'seed' gratings in samples prepared with different thicknesses. The grating spatial frequency is 500 lines/mm and the layer thicknesses are approximately 60 μm (solid), 130 μm (dotted-line), 190 μm (dashed line) and 240 μm (dotted line). Initial diffraction efficiency is approximately 1% for the two-beam grating.

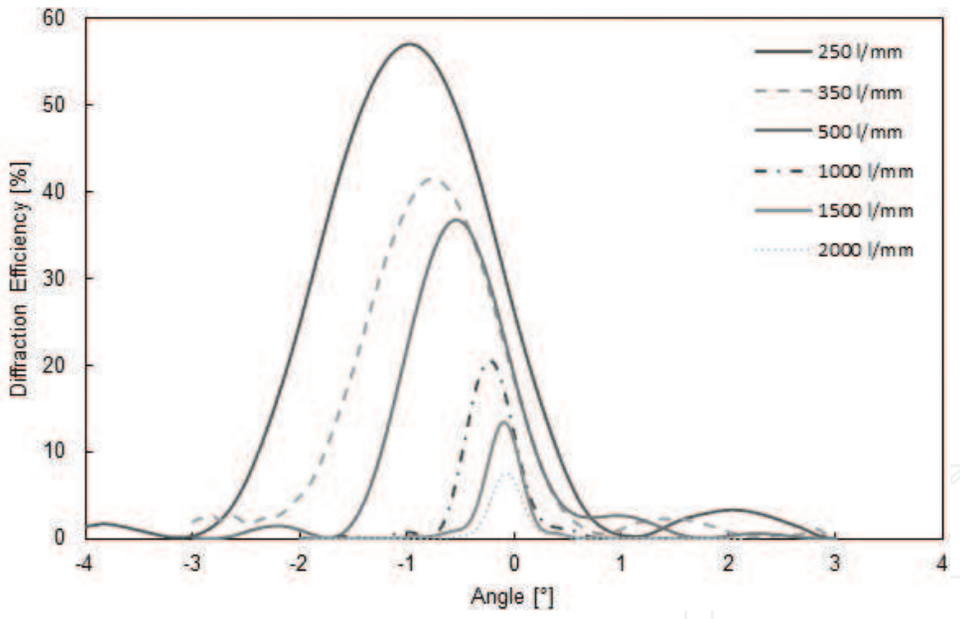

Figure 16. Bragg curves (the variation of diffraction efficiency with reading beam angle of incidence) for a series of gratings formed using the single beam process using different spatial frequency seed gratings. Layer thickness is approximately 140 μm.

beam to the weak diffracted beam during single-beam recording. It seems reasonable that this process will be more efficient when the fringe period is very much larger than the wavelength.

As well as the clear dependence of final on-Bragg diffraction efficiency on spatial frequency, the changes in the width of the Bragg curve are also obvious. In addition, we can see that the

shift in the position of the Bragg peak increases as the spatial frequency decreases and the magnitude of the effect increases.

5.2.4. Angular multiplexing of data using a one beam system

In some applications, it may be necessary to obtain a diffraction efficiency increase in one grating selected from a number of gratings angularly multiplexed in the same region of the photopolymer layer, without affecting its neighbours. The selectivity demonstrated in **Figure 14** implies that this should be possible.

In order to investigate if it would be possible to selectively boost one grating from a series, a layer of photopolymer 135 μm in thickness was used and five seed gratings of equal strength were angularly multiplexed into it. One of the gratings was then illuminated at its Bragg angle in order to increase its efficiency. For separations up to 1.8°, illumination caused a significant increase in the diffraction efficiency of gratings on either side of the intended grating. **Figure 17** shows the result for gratings 2° apart. Although there are only five seed gratings in these examples, the principle is demonstrated that one of a set of angularly multiplexed gratings, separated by 2°, can be enhanced by illuminating it at the appropriate angle with a single beam of light. Working with higher spatial frequency and thickness would be likely to allow smaller angular separations between neighbouring gratings.

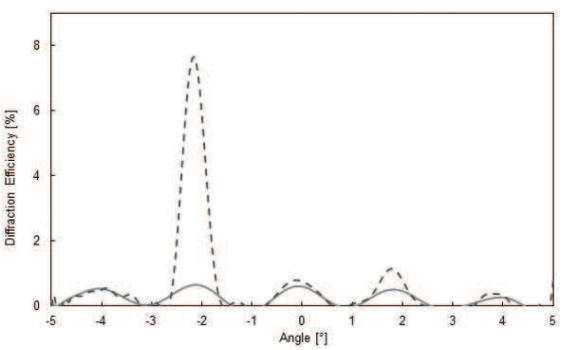

Figure 17. Variation of diffraction efficiency with the reading beam angle of incidence for a series of gratings, from which one individual grating has been enhanced by illuminating with a single on-Bragg beam of light. The angular separation between neighbouring gratings is 2°.

6. Conclusion

High efficiency diffractive optical elements have been recorded holographically with low spatial frequency. Three slanted gratings were successfully stacked using lamination and shown to increase significantly the range of angles from which light could be collected. However, positioning gratings in the path of the detector/cell meant that although light incident at large angles was coupled into the detector, an equivalent amount of light was deflected away from the detector at lower angles. When arranged off-axis, however, they increased the total light collected. The HOEs were then tested with a solar simulator and shown to improve the energy collected at a Si solar cell by up to 60% when used off-axis in pairs.

http://dx.doi.org/10.5772/67296

Modelling off-axis low spatial frequency focusing elements confirms that a range of gratings spatial frequencies and slant angles exists in the recorded elements and by simple geometry we can predict the grating spacing and slant angle at any point across the element and use coupled wave theory to predict the diffraction behaviour at a particular location. Good agreement is shown between theory and experiment and measurements made using phase contrast microscopic imaging of the photonic structure also agree closely.

A method of writing low spatial frequency holographic gratings with a single beam was also presented and shown to be capable of writing high diffraction efficiency gratings under unstable conditions. The technique is based on the exposure of very weak pre-recorded gratings to a single illuminating beam in order to write new high efficiency gratings in the photopolymer material. Strong spatial frequency dependence was shown. Diffraction efficiencies of 60% were obtained in just 30 sec with a 250 line/mm grating. With longer exposures up to 80% was achieved. The potential for angular multiplexing was shown by illuminating a single grating from among five multiplexed weak gratings and increasing its efficiency eightfold with a negligible effect on the other gratings.

In conclusion, these studies of low spatial frequency holographic optical elements have shown their potential for solar applications, their capacity to function as thick volume gratings and the success with which their microstructure can be controlled and modelled. Their particular potential for recording self-interference has also been exploited as a vibration-immune holographic recording method. The challenges that remain include modelling of the non-linear effects that occur during low spatial frequency holographic recording, development and modelling of more complex low spatial frequency elements and combinations of elements. Future work will focus on developing new diffractive elements and exploitation of these in practical applications.

Acknowledgements

The authors would like to acknowledge the IEO Centre's funding from Enterprise Ireland through its Commercialization Fund (which is co-funded by the European Union through the European Regional Development fund), the Dublin Institute of Technology's Fiosraigh Scholarship Fund, and the Irish Department of Education's Programme for Third Level Research Institutes Strand 1 scholarships.

Author details

Suzanne Martin*, Hoda Akbari, Sanjay Keshri, Dennis Bade, Izabela Naydenova, Kevin Murphy and Vincent Toal

*Address all correspondence to: suzanne.martin@dit.ie

Centre for Industrial and Engineering Optics, School of Physics, College of Sciences and Health, Dublin Institute of Technology, Dublin, Ireland

References

[1] H. Kogelnik. Coupled wave theory for thick hologram gratings. The Bell System Technical Journal. 1969; **48**(9):2909–47.

[2] P. Hariharan. Optical holography, principles techniques and applications. 2nd ed. New York: Cambridge University Press; 1996. 405 p.

[3] A. Bianco et al. The design of dispersing elements for a highly segmented, very wide field spectrograph. SPIE Proceeding. 2010; **7735**: 77357M-1. DOI: 10.1117/12.857689.

[4] J. Marín-Sáez, J. Atencia, D. Chemisana and M. V. Collados. Characterization of volume holographic optical elements recorded in Bayfol HX photopolymer for solar photovoltaic applications. Optics Express. 2016; **24**(6): 258–926. DOI: 10.1364/OE.24.00A720.

[5] H. Akbari. Investigation of photopolymer-based holographic optical elements for solar applications [thesis]. Dublin, Ireland: Dublin Institute of Technology; 2015.

[6] T. Mikulchyk, S. Martin and I. Naydenova. Investigation of the sensitivity to humidity of an acrylamide-based photopolymer containing N-phenylglycine as a photoinitiator. Optical Materials. 2014; **37**: 810–815. DOI: 10.1016/j.optmat.2014.09.012.

[7] H. Akbari, I. Naydenova and S. Martin. Using acrylamide-based photopolymers for fabrication of holographic optical elements in solar energy applications. Applied Optics. 2014; **53**: 1343–1353.

[8] S. T. L. Sam and A. P. T. Kumar. Design and Optimization of Photopolymer Based Holographic Solar Concentrators. AIP Conference Proceedings 1391, 2011; 248250, DOI: 10.1063/1.3646844.

[9] A. Ghosh, A. K. Nirala and H. L. Yadav. Dependence of wavelength selectivity of holographic PV concentrator on processing parameters. Optik—International Journal for Light and Electron Optics. 2015 Mar; **126**(6): 622–625.

[10] M. Hsieh, S. Lin, K. Y. Hsu, J. A. Burr and S. Lin. An efficient solar concentrator using volume hologram. Conference on Lasers and Electro-Optics. 2011; **1**: 4–5.

[11] D. Zhang, J. M. Castro and R. K. Kostuk. One-axis tracking holographic planar concentrator systems. Journal of Photonics Energy. 2011; **1**(1): 015505.

[12] J. Hung, P. S. Chan, C. Sun, C. W. Ho, W. Y. Tam. Doubly slanted layer structures in holographic gelatin emulsions: solar concentrators. Journal of Optics. 2010; **12**(4): 045104.

[13] R. K. Kostuk, J. Castillo, J. M. Russo and G. Rosenberg G. Spectral-shifting and holographic planar concentrators for use with photovoltaic solar cells. SPIE Proceeding. 2007; **6649**: 66490I–66490I–8.

[14] B. Sreebha, V. P. Mahadevan Pillai PTAK. Development of a window holographic lens to utilize solar energy, advances in optical science and engineering. V. Lakshminarayanan, I. Bhattacharya, editors. New Delhi: Springer India; 2015.

[15] G. Bianco, M. A. Ferrara, F. Borbone, A. Roviello, V. Striano, G. Coppola. Photopolymer-based volume holographic optical elements: design and possible applications. Journal of the European Optical Society—Rapid publications. 2015; **10**: 15057. DOI: 10.2971/jeos.2015.15057.

[16] I. Naydenova, H. Akbari, C. Dalton, M. Yahya so M. Ilyas, C. Pang Tee Wei, V. Toal and S. Martin. Photopolymer holographic optical elements for application in solar energy concentrators. In: E. Mihaylova, editor. Holography—basic principles and contemporary applications. InTech; 2013. DOI: 10.5772/55109.

[17] S. Altmeyer, Y. Hu*, P. Thiée, J. Matrisch, M. Wallentin and J. Silbermann. Multiplexing of transmission holograms in photopolymer. DGaO Proceedings ISSN: 16148436; 2013; urn:nbn:de:02872013B0099

[18] H. Akbari, I. Naydenova, L. Persechini, S. M. Garner, P. Cimo and S. Martin, Diffractive optical elements with a large angle of operation recorded in acrylamide based photopolymer on flexible substrates. International Journal of Polymer Science. Vol. **2014**; 2014.

[19] M. Ortuño, F. Fernández, S. Gallego, A. Beléndez and I. Pascual. New photopolymer holographic recording material with sustainable design. Optics Express. 2007; **15**(19): 12425–12435.

[20] I. K. Baldry, J. Bland-Hawthorn and J. G. Robertson. Volume phase holographic gratings: polarization properties and diffraction efficiency. Astronomical Society of Pacific. 2004; **116**(819): 403–414.

[21] N. Kukhtarev, G. Dovgalenko, G. C. Duree, Jr., G. Salamo, E. J. Sharp, B. A. Wechsler and M. B. Klein. Single beam polarization holographic grating recording. Physical Review Letter. 1993; **71**(26): 4330.

[22] S. Naruse, A. Shiratori and M. Obara. Holographic memory with one-beam geometry in photorefractive crystal. Applied Physics Letter. 1997; **71**(4).

[23] H. Mitsuhashi and M. Obara. Compact holographic memory system using a one-beam geometry in a photorefractive crystal. Applied Physics Letter. 2001; **79**(7).

[24] H. F. Yau, J. P. Liu, H. Y. Lee and Y. Z. Chen. Single beam one-way imaging through a thick dynamic turbulent medium. Applied Optics. 2006; **45**(19): 4625.

[25] C. S. Chiang, M. T. Shiu and W. H. Wu. Multiple-hologram recording with one-beam encoding. Optics Express. 2012; **20**(7): 6897.

[26] N. Kukhtarev and T. Kukhtareva. Single beam dynamic holographic interferometry. In: Photonic Fiber and Crystal Devices: Advances in Materials and Innovations in Device Applications IV; August 17th; SPIE; 2010. 77810H p.

[27] N. V. Kukhtarev, T. V. Kukhtareva and A. Chirita. Holographically amplified interferometry with coherent fringe projection for the oil on the water remote sensing and characterization. In: Photonic Fiber and Crystal Devices: Advances in Materials and Innovations in Device Applications VII; September 25th; SPIE; 2013. 88471J p.

[28] H. Horimai, X. Tan and J. Li. Collinear holography. Applied Optics. 2005; **44**(13): 2575.

[29] S. Martin, C. A. Feely, J. T. Sheridan and V. Toal. Applications of a self-developing photopolymer material: holographic interferometry and high efficiency diffractive optical elements. Optical Memory and Neural Networks. 1998; **7**(2): 79.

[30] B. L. Booth. Photopolymer material for holography. Applied Optics. 1975; **14**(3): 593.

[31] S. Martin, D. Bade, I. Naydenova and V. Toal. A single beam data writing process for holographic data storage. In: K. Kurtis, editor. IEEE LEOS Optical Data Storage; 10–13 May; Florida. IEEE; 2009. TuC5 p.

[32] M. R. Gleeson, J. V. Kelly, F. T. O'Neill and J. T. Sheridan. Recording beam modulation during grating formation. Applied Optics. 2005; **44**: 5475–5482.

[33] M. Kveton, A. Havranek, M. Skere and P. Fialia. Real-time measurements of diffraction grating growth in photopolymer recording materials. EPJ Web of Conferences. 2013; **48**: 00013. DOI: 10.1051/epjconf/20134800013.

[34] M. Ulibarrena, L. Carretero, R. Madrigal, S. Blaya and A. Fimia. Nonlinear effects on holographic reflection gratings recorded with BB640 emulsions. Optics Express. 2003; **11**(16): 1906–1917. DOI: 10.1364/OE.11.001906.

[35] A. Murciano, S. Blaya, L. Carretero, P. Acebal, M. Pérez-Molina, R. F. Madrigal and A Fimia. Analysis of nonuniform transmission gratings recorded in photopolymerizable silica glass materials. Journal of Applied Physics. 2008; **104**: 063109. DOI: 10.1063/1.2980332.

[36] I. Naydenova, R. Jallapuram, R. Howard, S. Martin and V. Toal. Investigation of the diffusion processes in self-processing acrylamide-based photopolymer system. Applied Optics. 2004; **43**(14): 2900.

[37] T. Babeva, I. Naydenova, R. Jallapuram, R. Howard, S. Martin and V. Toal. Study of the photoinduced surface relief modulation in photopolymers caused by illumination with a Gaussian beam of light. Journal of Optics. 2010; **12**: 124011.